Electromigration Performance Improvement of Metal Heaters for Si Photonic Ring Modulators

David Coenen[1,2], Kristof Croes[2], Artemisia Tsiara[2], Herman Oprins[2], Veerle Simons[2], Olalla Varela Pedreira[2], Yoojin Ban[2], Joris Van Campenhout[2], Ingrid De Wolf[1,2]
[1]Dept. Materials. Eng. KU Leuven, Leuven, Belgium, [2]imec, Kapeldreef 75, Leuven, Belgium
David.Coenen@imec.be

***Abstract*—Ring-based, resonant Si photonic (SiPho) devices are temperature sensitive and require thermal tuning for stable operation, which is accomplished with integrated metallic heaters. This paper investigates the combined electromigration (EM) and thermal performance of tungsten (W) heaters using calibrated electro-thermal finite element models. The current injectors that are used to supply the current to the heater are a known weak spot for electromigration. The presented modelling study shows the conflicting design requirements for optimal thermal performance and optimal EM performance, which results in the need of a careful trade-off, supported by experimental reliability data. Based on modelling results, new device designs are proposed with significant performance increase. Lastly, a new methodology is introduced which allows to predict the lifetime of the W-heaters, given specific operating conditions such as ambient temperature and required phase shift.**

***Index Terms*—Electromigration, Silicon Photonics, thermal modelling**

I. Introduction

SILICON photonic transceivers for optical IO using ring based architectures and wavelength division multiplexing (WDM) are of interest because of their compact footprint and energy-efficient operation [1], [2]. At the transmitter side, ring modulators can be used for electro-optic modulation of light. At the receiver side, ring resonators can be used as wavelength-specific filters for demultiplexing WDM signals. These devices have in common that their operation is based on the resonance of light within the ring structure. However, this comes with additional challenges. Because of the high thermo-optic coefficient of Si ($1.8 \cdot 10^{-4}$ 1/K) [3], the resonance wavelength is temperature sensitive and if there is a mismatch between the resonance wavelength and the wavelength used for the channel, the quality of the communication link degrades. To solve this temperature-sensitivity, the resonant devices are equipped with an integrated metal heater close to the waveguide (WG) which allows for accurate temperature control (i.e. thermal tuning) [4]. The layer stack of the SiPho die is shown in Fig.1, where the W-heater (MHD) is located above the Si waveguide. The current is supplied to the heater by the Cu injector. The metal contacts to the p-n junction waveguide (Fig.1, right) are emitted from the 3D view (left) for clarity, they are in fact included in the model. By applying current to the metal heater, the device will heat up by Joule heating and consequently the temperature of the waveguide can be controlled by changing the input current.

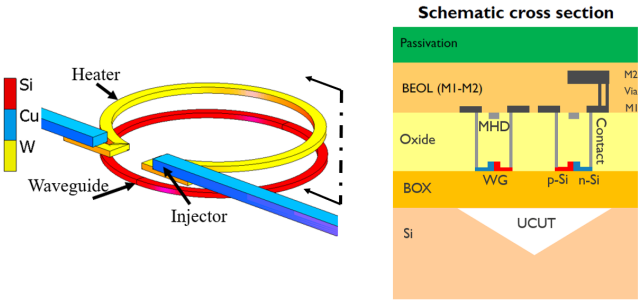

Fig. 1. Basic components of a ring modulator (left): Si waveguide, W-heater and Cu injector. Cross-section of SOI layer stack (right). UCUT = substrate undercut, WG = waveguide, MHD = metal heater, BEOL = back end of line, M1 = metal one, M2 = metal two

During the operation of the W-heaters, high current densities are required in order to generate sufficient Joule heating. This exposes the structure to an electromigration (EM) risk at the connection between the W and the Cu close to the point where the electrons enter the Cu. This connection will be further referred to as the (current) injector. Electromigration is driven by the momentum transfer between the electrons and metal atoms, which can diffuse. High current and temperature will enhance this process. If the electromigration is allowed to continue for an extended period, voids can nucleate and grow in this injector which ultimately destroys the connection. In previous work [7], it is shown for straight W-heaters (in Mach-Zehnder modulators or thermo-optic phase shifters [8]), that EM occurs at the injector. The analysis of the EM activation energy suggested that the temperature close to the void is equal to the ambient temperature. However, as ring-based W-heaters are much more compact, the injector is located closer to the hot part of the device. This results in a temperature at the location of the void which is higher than ambient, complicating the analysis. Thermal modelling will be used to accurately simulate this temperature and this information will be used for lifetime prediction.

The goal of this research is to propose metallic ring heaters for SiPho devices which are both reliable and energy efficient. This is done by analyzing experimental

results, calibrating finite element models and finally using the models for exploring improved designs. In Section II the different requirements for optimal thermal design and optimal reliable design will be discussed, along with the methodology for combined thermal and EM assessment. In Section III experimental results are presented, which are used for model calibration and validation. The experiments consist of Joule heating measurements on the W-heaters, electro-optic characterization of the waveguide and device EM-stress-tests at elevated temperature. With the validated electro-thermal finite element (FE) models, device designs are proposed with improved thermal and EM performance. In Section IV the device performance is discussed and lifetime predictions are made, based on experimental data and extrapolation models.

II. Methodology

The design of the W-heater and its current injector (Fig.1) is subjected to conflicting requirements, which will be further elaborated in this section. The main functionality of the heater is to increase the waveguide temperature. This requires electrical input power and the figure of merit (heater efficiency) is the average waveguide temperature normalized by heater power $\eta_h = T_{wg}/P$. For maximal energy efficiency, the waveguide temperature has to be as high as possible, and the power to achieve this as low as possible. The waveguide temperature is linked to the heater temperature through the coupling coefficient C_{wg} (Eq.1). There are two ways to increase the waveguide temperature as shown in Eq.1: increase the WG-heater coupling C_{wg} or increase the heater temperature. As soon as the heater temperature is increased, the injector temperature increases as well through the coupling between both C_{inj} (Eq.2).

$$C_{wg} = \frac{T_{wg}}{T_{heater}} \tag{1}$$

$$C_{inj} = \frac{T_{inj}}{T_{heater}} \tag{2}$$

Because the coupling coefficients (Eq.2, Eq.1) are fixed for a specific design, the injector temperature is coupled to the waveguide temperature by $T_{inj}[^\circ C/mW] = \frac{C_{inj}}{C_{wg}} \cdot T_{wg}$. The injector however, should be kept at a low temperature due to EM-demands, which conflicts with the main purpose of the heater. Here a trade-off emerges: the injector should be kept at a low temperature while the waveguide is at a high temperature. In this paper we will investigate how the physical design can be optimized in order to limit $\frac{C_{inj}}{C_{wg}}$, which minimizes the injector temperature while maintaining a high waveguide temperature.

The heater efficiency η_h is expressed in units of °C/mW for thermal analysis and can be converted to nm/mW, which is the resonance wavelength shift expressed in nm normalized by heater power P (Eq.3). This conversion is useful for comparing thermal modelling results with experimental data (Section III.A), and can be expressed as follows [9]:

$$\frac{dT}{dP} = \frac{d\lambda}{dP} \frac{\lambda}{FSR \cdot 2\pi r \cdot \frac{dn_{eff}}{dT}}, \tag{3}$$

where $\lambda = 1304\ nm$ is the wavelength of light in O-band, $r = 5\ \mu m$ the waveguide radius, FSR the free spectral range and $dn_{eff}/dT = 1.95 \cdot 10^{-4} K^{-1}$ the thermo-optic coefficient of the effective refractive index of the fundamental mode in the waveguide [9].

$$FSR = \frac{\lambda^2}{n_g 2\pi r} = 13.37\ nm, \tag{4}$$

where $n_g = 4.088$ is the group index. The above values are valid for a Si waveguide (cross section 450 x 225 nm^2) with SiO_2 cladding and are obtained by optical simulation in Lumerical. The FSR is also determined experimentally as the wavelength spacing between two consecutive resonances of the RM: 13.41±0.16 nm, which matches well with the theoretical value.

In order to compare the performance of different designs, their temperature and current is evaluated at the same operating point: full FSR phase shift. The required power for FSR phase shift can be calculated as:

$$P_{FSR} = \frac{FSR}{d\lambda/dP} \tag{5}$$

P_{FSR} should be minimized in order to minimize thermal tuning energy spending. Once P_{FSR} is known the corresponding injector temperature can be calculated:

$$T_{inj}[^\circ C] = \frac{C_{inj}}{C_{wg}} \cdot P_{FSR} \cdot T_{wg} \tag{6}$$

A. Methodology for combined thermal and EM assessment

The methodology starts with the experimental characterization of two different ring modulator designs, more specifically the thermal resistance of the heaters is measured. The ring radius is 5 μm and the W-heater width is 600 nm for both designs. The main difference between design 1,2 is the current injector and the RM Cu connections in the BEOL layers (Fig.2). Design 1 has a relatively simple current injector where a Cu block is placed on top of the heater extension. Design 2 on the other hand has a more elaborate heater extension with three fingers. This allows for a larger Cu volume in the injector, extending the electromigration liftetime. With the obtained measurement data, electro-thermal finite element models are calibrated. Based on the simulation results, a new design is proposed and tested through simulation. Device performance is extracted from the models, mainly being the temperature of the injector, heater and waveguide. These data can be used to predict the lifetime of the devices using Black's equation (Eq.7), assuming electromigration failure. In order to do this, experimental data of stress-tests of design 1 are used as a starting point from where extrapolation is possible. The methodology is summarized in Fig.3. Black's equation is:

$$MTTF = \frac{c_t}{j^n} e^{\frac{E_a}{k_b T}}, \tag{7}$$

where $MTTF$ is the mean time to failure, c_t is a model constant, j is the current density, n is the current scaling factor, E_a is the activation energy for electromigration in Cu, k_b is the Boltzmann constant and T the temperature at

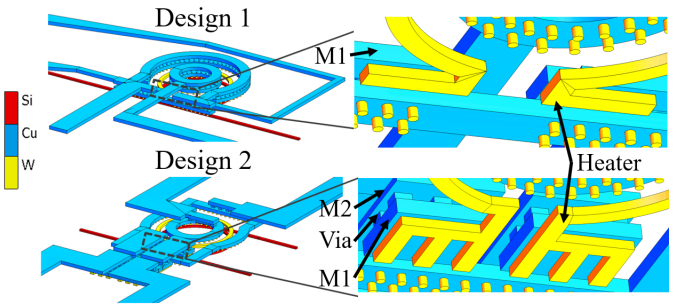

Fig. 2. Design 1&2 with detailed bottom-view of current injector. M1 Cu layer, via layer and M2 Cu layer are indicated.

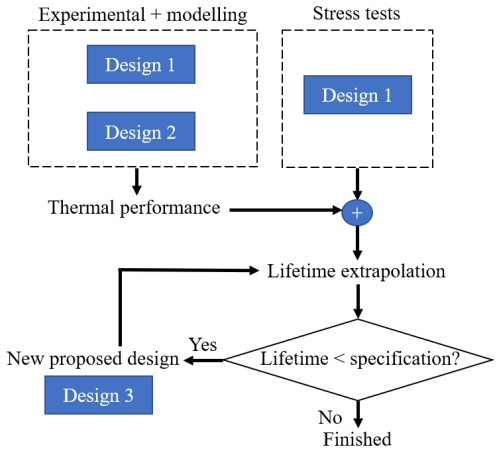

Fig. 3. Methodology used in this work

the location of the void. In this work we assume n=1.5 as the mid-point between void growth (n=1) and void nucleation (n=2). The reason for this approach is that, since a high Joule heating is induced during normal operation, standard electromigration test approaches where the Joule heating during electromigration testing is kept low are not applicable for our case. It is well-known in literature that a high Joule heating will induce an artificially, temperature dependent, high n-factor which would in its turn lead to artificially optimistic lifetime predictions. Hence, we could not use the n-factor obtained from our electromigration tests. Since from electromigration physics it is known that n is somewhere between 1 (void growth) and 2 (void nucleation), we opted for the choice of n=1.5. For the activation energy we assume $E_a = 0.85\,\text{eV}$ [7], [13], this value is also obtained in internal reference electromigration tests. Using Eq.7, the ratio of the lifetimes of devices at different temperatures can be expressed as Eq.8 and the ratio of lifetimes for different current densities as Eq.9.

$$AF_{temp} = e^{\left[\frac{E_a}{k_b}\cdot\left(\frac{1}{T_2}-\frac{1}{T_1}\right)\right]} \tag{8}$$

$$AF_{current} = \left[\frac{j_1}{j_2}\right]^n \tag{9}$$

Here AF stands for acceleration factor: accelerating the electromigration failure. The total lifetime ratio or gain can be found by multiplying the temperature and current density ratio (Eq.10).

$$AF_{total} = AF_{current}\cdot AF_{temp} = \left[\frac{j_1}{j_2}\right]^{1.5}\cdot e^{\left[\frac{0.85}{k_b}\cdot\left(\frac{1}{T_2}-\frac{1}{T_1}\right)\right]} \tag{10}$$

This total gain is an important metric to calculate, as this will allow to extrapolate the lifetime at stressed conditions to regular conditions. The current ratio j_1/j_2 can also be expressed in terms of (void) temperatures by using the relationship in Eq.11.

$$\frac{j_1}{j_2} \sim \frac{P_1^{1/2}}{P_2^{1/2}} \sim \frac{T_1^{1/2}}{T_2^{1/2}} \tag{11}$$

For this relationship to hold, it is assumed that the system is linear and thus the material properties stay constant during the heating of the device. Solving Eq.10 for T_2 will be useful for predicting how much wavelength shift can be obtained, given the constraint of a minimum required lifetime. The analytical solution to this equation is not obtainable due to its highly non-linear nature, however the expression can be evaluated numerically using the scientific computing package SciPy [14]. The current term in Eq.10 scales with temperature as $AF_{current} = (T_1/T_2)^{n\cdot 0.5}$, so with exponent 0.75. This is much less compared to the exponential scaling of the temperature term (Eq.8). For this reason, we can approximately assume $AF_{curr} \approx 1$ which simplifies the analytical solution of Eq.10 to:

$$T_2 = \frac{E_a}{k_b \cdot ln\left(AF_{total}e^{E_a/(T_1 k_b)}\right)} \tag{12}$$

where T_2 is the modelled temperature at the location of the void at normal operating conditions and T_1 at the accelerated aging condition. The lifetime of new designs were estimated in the following way (Section IV.D): first AF_{total} is calculated. For example, if the lifetime has to be extended from 150 hours to 5 years, approximately AF_{total} ~292 is used. Then T_2 is calculated, which can be interpreted as the maximum allowed temperature at the location of the void for obtaining the extended lifetime. Finally, this temperature is used in Eq.6 for the determination of the waveguide temperature, which is directly linked to the obtainable optical phase shift of the ring (Eq.3).

III. Experiments

In the first subsection the W-heater temperature measurements for both ring modulator designs are discussed. In the second subsection, the devices are measured electro-optically by measuring the induced resonance wavelength shift for an applied power to the heater. This induced shift can be related to the average waveguide temperature increase (Section I.C). The goal of the measurements is to calibrate the thermal RM models.

A. Characterization of design 1,2

Of design 1, 12 devices are measured and of design 2 5 devices are measured. The W-heater temperature is determined by using the Temperature Coefficient of Resistance (TCR) of

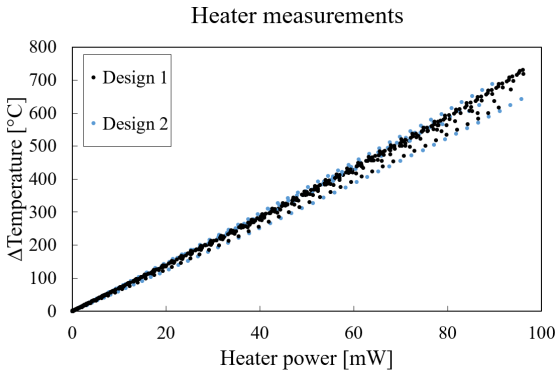

Fig. 4. Heater temperature measurement

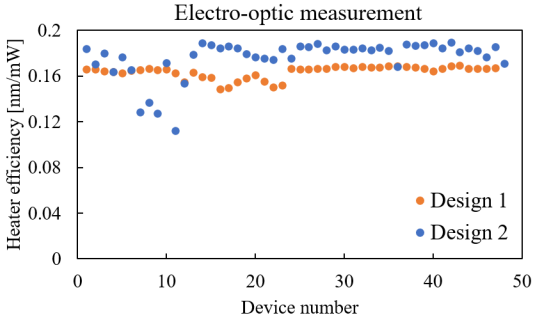

Fig. 5. Electro-optic device characterization of design 1 and 2

W during Joule heating measurements. The heater resistance is temperature sensitive $R(T) = R_0 + TCR \cdot R_0 \cdot T$ and by measuring the resistance change after applying heater power, the average temperature increase can be calculated as $\Delta T = \Delta R/(TCR \cdot R_0)$. In Fig.4 the experimental results are shown. There is no significant difference between design 1 and design 2. The normalized, average heater temperature from the experiments is 7.03 °C/mW.

The devices are also characterized electro-optically. The measurement result of 48 different devices are shown in Fig.5: after applying power to the heater, the induced resonance wavelength shift is measured. The spread on the data is small, except some outlying datapoints. To accommodate the outliers, the median value 0.183±0.019 nm/mW is thus selected for further analysis of design 2 heater efficiency. The variability on the measurements on design 1 is smaller thus the average is used for further analysis 0.165±0.005 nm/mW.

B. Reliability data on design 1

The devices with design 1 are stressed at elevated ambient temperature until failure. Note that, as opposed to choosing more standard electromigration structures, we have chosen to use a real design as electromigration test structure. We have done this for two reasons. 1) Because the temperature of the location where the void happens is highly dependent on the chosen test structure. A standard electromigration structure could have different temperatures at the location of the void and could thus lead to completely different failure times. 2) The induced thermal gradient during stress is highly dependent

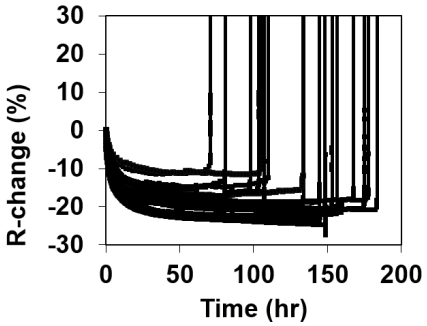

Fig. 6. Electromigration data on design 1 for full FSR phase-shift

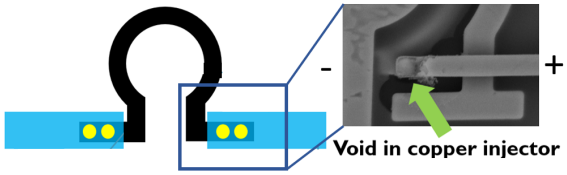

Fig. 7. Microscope picture of void location in the Cu located at the anode

on the chosen test structure. As a thermal gradient will be present during normal operation (Fig.8), a test structure that induces similar thermal gradients is crucial for a reliable lifetime assessment. Given the above two reasons, we believe that the choice of a test structure which as close as possible mimics the real device is more appropriate than a standard electromigration test structure. The reliability of the devices is expressed as $t_{50\%}$, which is the lifetime where the cumulative failure rate reaches 50%. The stress conditions are an ambient temperature of 150°C and current required for full FSR phase shift. Stress-test results are shown in Fig.6. For $T_a = 150$°C, $t_{50\%} \approx 120\ h$. In Fig.7 the failure location is indicated, and the void in the injector is highlighted. As expected, the void is happening in the injector at the location where the electrons enter the Cu. At this location the W-heater acts as a flux divergence point. This indicates that the EM reliability will be determined by the temperature at this location in the injector.

IV. Discussion

A. Modelling methodology and calibration

The SiPho ring modulator with W-heater is modelled by finite element electro-thermal simulation, using the software MSC Marc [15]. Details on the calibrated thermal modelling approach for ring modulators with and without undercut Si substrate (UCUT) can be found in [9]. The thermal boundary conditions correspond to probestation testing: convective heat transfer on the top surface ($h = 20\ W/m^2K$) and an isothermal bottom face. The die sidewalls are adiabatic. The simulation result of injector temperature for both designs is shown in Fig.8 The measured heater efficiency η_h for design 2 is 0.183 nm/mW (Fig.5), the model has a heater efficiency of 3.07°C/mW which corresponds to 0.205 nm/mW. The average W-heater temperature from simulation is 6.44-7.19°C/mW for design 2 and 1 respectively. The experimentally measured

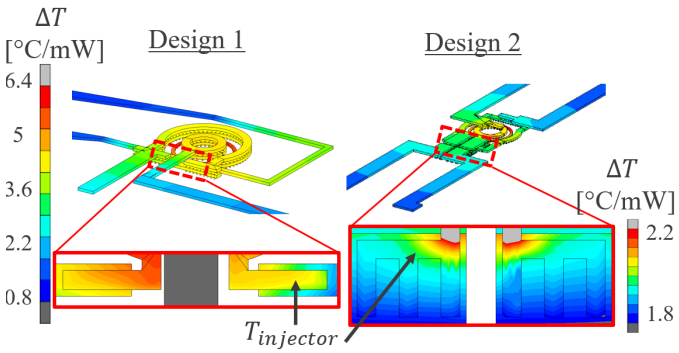

Fig. 8. Simulation result of design 1&2. Adjusted scale for injector temperatures, T_{inj} extracted as average temperatures on W-Cu contact interface

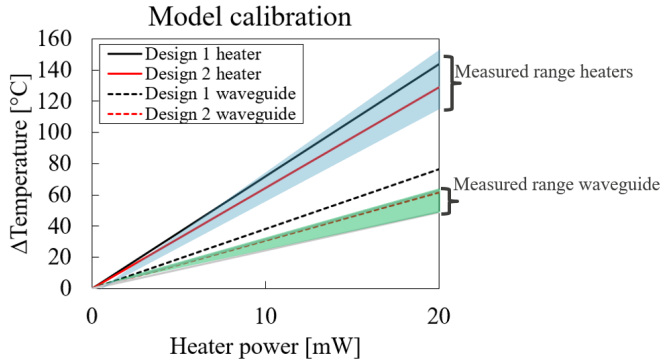

Fig. 9. Model calibration: black and red lines show simulation results, indicated ranges show measured interval.

values (Fig.4) are in the range 5.85-7.73°C/mW (minimum and maximum measured values). The simulation model matches well with the experimental data. The comparison between modelling and experimental data is shown in Fig.9, and the model is considered validated.

B. Device performance

Electro-thermal finite element simulation results are summarized in Table I. From a thermal point of view T_{wg} should be as high as possible, in order to reach high temperature in the waveguide for minimal input power. From reliability point of view, T_{inj} should be as low as possible in order to reduce risk of electromigration failure. As expressed in Section II, both requirements are conflicting but they can be combined in a single performance metric: C_{inj}/C_{wg} which should be minimized. The performance of design 1 and design 2 is shown in Table I. The injector of design 2 has a much lower coupling C_{inj} compared to design 1, limiting the injector temperature and hence extending its lifetime. However, the heater efficiency T_{wg} is lower compared to design 1, indicating that more electrical power is required to obtain the same phase shift. This power increase is achieved by increasing input current, lowering the device lifetime. Overall, the combined performance metric C_{inj}/C_{wg} of design 2 is already improved compared to design 1. It is clear that there is still room for optimization, given the simulation results of both designs. In Section IV.C, a list of

TABLE I
DEVICE SIMULATION RESULTS: TEMPERATURES ARE AVERAGES

	Design 1	Design 2	Design 3	Unit
	No UCUT			
T_{heater}	7.190	6.440	8.776	[°C/mW]
T_{wg}	3.820	3.070	4.250	[°C/mW]
T_{inj}	4.867	2.892	3.651	[°C/mW]
C_{wg}	0.531	0.477	0.484	[-]
C_{inj}	0.677	0.449	0.416	[-]
C_{inj}/C_{wg}	1.275	0.941	0.859	[-]
	UCUT			
T_{heater}	12.983	9.322	16.011	[°C/mW]
T_{wg}	10.010	6.610	11.954	[°C/mW]
T_{inj}	9.711	5.089	8.838	[°C/mW]
C_{wg}	0.771	0.709	0.746	[-]
C_{inj}	0.748	0.546	0.552	[-]
C_{inj}/C_{wg}	0.970	0.770	0.739	[-]

possible improvements is given and a more optimal design 3 is discussed.

The removal of Si substrate below the ring modulator has been shown to increase the heater efficiency with a factor 3 [9]–[12] due to the increased thermal isolation. Hence it is a very appealing design choice, but the question remains what its impact is on the reliability of the device. The simulation results with UCUT are summarized in Table I (bottom). Adding UCUT increases the heater efficiency with a factor 2.15-2.81, greatly reducing the required current for FSR phase shift. Secondly, the coupling coefficients are influenced as well. The waveguide coupling C_{wg} increases with a factor 1.45-1.57, which is beneficial for limiting the heater and injector temperature for a given waveguide temperature. Thirdly, the injector coupling C_{inj} increases with a factor 1.10-1.32 which is a drawback of introducing UCUT. Because of this vertical isolation, the heat spreads more laterally and consequently the injector coupling is increased. Because the positive effects outweigh this negative effect, using UCUT will always increase the device lifetime (Fig.11).

C. Design improvements

The idea in this section is to take the best of both designs and combine this in a new design 3. Device characteristics of design 2 which will be kept, focussing on low C_{inj}:

1) Injector design with multiple fingers
2) Injector further from ring center

Design changes focussing on high T_{wg}:

1) Taper the heater connection
2) Move heater connection to M2, from M1
3) Redesign RF-connections: decrease width and move to the same side

By tapering the heater connections, parasitic power loss in the connections is minimized as the resistance of the Cu line is inversely proportional with the cross-sectional area $R \sim A^{-1}$. The Cu connections to the device effectively form a heat sink, because of their high thermal conductivity compared to SiO_2 in which the device is embedded. In order to increase the heater efficiency, heat losses by conduction through the metal lines should be avoided. This can be achieved by the design

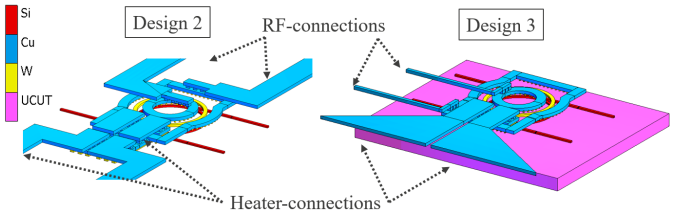

Fig. 10. Design 3

changes mentioned above. First, the heater connection is fully moved to M2 to increase the physical distance between the metal and the center of the ring. Secondly, the width of the RF-connections is reduced and they are moved to the same side. The increased resistance of the RF-connections is less of a concern because they require less current than the heater. There is a limit on the line width related to the RC time constant which is not further elaborated here. The performance of design 3 is shown in Table I: the heater efficiency ($\eta_h \sim T_{wg}$) has increased with a factor 1.38 compared to design 2, the injector coupling decreased with a factor 0.93 and the combined performance metric C_{inj}/C_{wg} decreased with a factor 0.91, which are all desired and intended effects.

D. Lifetime prediction

Using the methodology explained in Section I.C, the lifetime of the different designs can be estimated. This is based on experimental data available from stress tests of design 1 at elevated temperature (Section II.B), which can be extrapolated to standard operating conditions. An important assumption is made here: the model constant c_t from Black's equation (Eq.7) is kept the same for all designs. This introduces a modelling error: the different injector geometries will result in different constants. For example, design 2 and 3 have injector fingers which adds redundancy and allows for a higher void volume prior to failure, which is not taken into account in the lifetime estimation. In other words, the calculated lifetimes of design 2,3 are worst-case estimates. The threshold for device electromigration reliability is chosen as a lifetime of 5 years under continuous operation and at most 50% of the devices fail ($t_{50\%} = 5$ years). The obtainable phase shift is calculated in function of ambient temperature (Fig.11) for the different designs and their UCUT variant. Any operating condition below the 5-year line will meet the reliability specification. As expected, in order of increasing reliability: design 1, design 2, design 3. The same holds for the variants with UCUT. Design 3 with UCUT can operate under full FSR phase shift for ambient temperatures up to 100°C.

Previous lifetime results discussed in this paper are obtained by the numerical solution of Eq.10. Alternatively, instead of solving Eq.10 for injector temperature and hence phase shift, it can simply be solved for the total lifetime gain AF_{tot}. Using this method, the lifetime of the device can be calculated for all different combinations of phase shift and

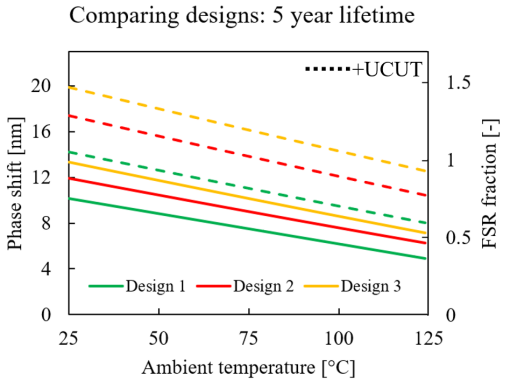

Fig. 11. Obtainable phase shift without exceeding the 5 year lifetime reliability specifications as a function of ambient temperature for different evaluated designs.

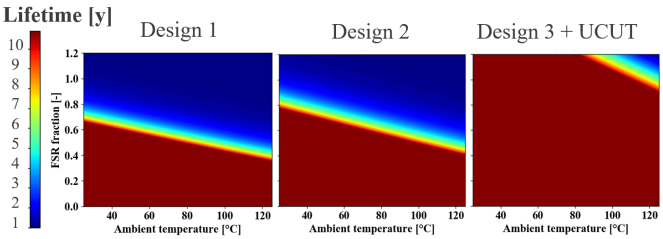

Fig. 12. Lifetime prediction of different designs

ambient temperature (Fig.12). All dark-red operating points visible in this figure have a lifetime of 10+ years.

V. Conclusion

Metal heaters for Si photonics applications consume a considerable amount of power whilst at the same time being a bottleneck for device reliability due to electromigration failure. The combined thermal and electromigration performance of two different ring heater designs is investigated in detail. From experimental characterization and numerical simulation strong and weak aspects of each design are identified. The temperature of the current injector needs to be limited in order to guarantee reliability specifications, while at the same time the temperature of the photonic waveguide needs to be as high as possible for energy efficiency purposes. This creates a design trade-off: optimal thermal design differs from optimal reliability design. Based on modelling analysis, heater design improvements are proposed and tested through simulation. By extrapolating device lifetime from stress tests to standard operating conditions, it is shown that the improved design can reliably operate under full FSR phase shift for at least 5 years.

Acknowledgment

This work was carried out as part of imec's industry affiliation R&D program "Optical I/O".

References

[1] Ph. Absil et al., "Reliable 50Gb/s silicon photonics platform for next-generation data center optical interconnects," *Electron Devices Meeting (IEDM)*, 2017.

[2] M. Rakowski et al., "Hybrid 14nm FinFET - Silicon Photonics Technology for Low-Power Tb/s/mm2 Optical I/O," *Symposium on VLSI Technology Digest of Technical Papers*, 2018.

[3] L. Pavesi, D.J. Lockwood, "Silicon Photonics III: Systems and Applications," *Springer*, 2016.

[4] S. Agarwal, "CMOS Circuitry for the Wavelength Locking of a Ring-based Silicon Photonics Transmitter," *Ph.D. Thesis, KU Leuven*, 2018.

[5] S. Beyne, O.V. Pedreira, H. Oprins, I. De Wolf, K. Croes, "Electromigration Activation Energies in Alternative Metal Interconnects," *IEEE Transaction on Electron Devices*, 2019.

[6] B. Li, T. D. Sullivan, T.C. Lee, D. Badami,"Reliability challenges for copper interconnects,"*Microelectronics Reliability*, Vol.44 (3), p.365-80, 2004.

[7] K. Croes et al., "Understanding EM-degradation mechanisms in metal heaters used for Si Photonics applications," *IEEE International Reliability Physics Symposium (IRPS)*, 2019.

[8] Q. Fang. et al., "Ultralow Power Silicon Photonics Thermo-Optic Switch With Suspended Phase Arms," *IEEE Photonics Technology Letters*, Vol. 23, No. 8, 2011.

[9] D. Coenen et al., "Thermal modelling of Silicon Photonic Ring Modulator with Substrate Undercut," *IEEE Journal of Lightwave Technology*, 2022 (*Accepted*).

[10] A. Masood et al., "CMOS-compatible Tungsten Heaters for Silicon Photonic Waveguides," *9th International Conference on Group IV Photonics*, 2012.

[11] A. Masood et al., "Comparison of heater architectures for thermal control of silicon photonic circuits," *10th International Conference on Group IV Photonics*, 2013.

[12] I. Shubin et al., "Integration, processing and performance of low power thermally tunable CMOS-SOI WDM resonators," *Optical and Quantum Electronics*, Vol.38, 2012.

[13] C. K. Hu, R. Rosenberg, K. Y. Lee, "Electromigration path in Cu thin-film lines," *Applied Physics Letters*, Vol. 74 (20), 1999.

[14] P. Virtanen et al., "SciPy 1.0: Fundamental Algorithms for Scientific Computing in Python", *Nature Methods*, Vol. 17, p.261-272, 2020.

[15] MSC-Marc, http://www.mscsoftware.com/product/marc